MJHES (2014) 4 (1), 13～22

【Original investigation】

The external force model for determining the frontal plane knee loading pattern –Implication for the mechanism of non-contact anterior cruciate ligament injury–

Issei Ogasawara[1)], Shumpei Miyakawa[2)], Shigeyuki Wakitani[1)]

Abstract

This study proposes a simple model for predicting the external knee adduction-abduction moment, which is a key mechanism of anterior cruciate ligament (ACL) injury. We simplified the Newton-Euler's equation of motion by omitting its dynamic terms, since the experimental trial revealed that the contribution of the dynamic terms became negligible relative to the external force term during landing impact phase. The experimental data also showed that the external force term precisely predicted the knee adduction-abduction moment which was calculated by the Newton-Euler's equation of motion. This result means that the knee loading pattern during impact activity is largely determined by the external force and if the lower limb orientation with respect to the ground reaction force (GRF) is inappropriate, knee would experience a large abduction loading. Next, we estimated GRF and its acting point from the measured kinematic data aimed at predicting knee loads without using a force plate data. The result indicated that the moment calculated by the external force model using estimated GRF broadly predicted the profile of the Newton–Euler method, but was less precise during impact phase. As an implication for the mechanism of non contact ACL injury, the specific landing motions which can especially increase the knee abduction loading were introduced through model consideration.

key words：External force term; Anterior cruciate ligament injury; Risk evaluation; Knee abduction moment; Zero-moment point

Ⅰ. Introduction

The anterior cruciate ligament (ACL) is frequently injured during impact activities such as jump landing or side cut motion.[1, 2] The forcefully abducted knee position at the moment of injury[3] implies that a large knee abduction moment is one of a main mechanism of this injury. An epidemiological study revealed that the population exhibiting increased knee abduction moment has a higher rate of ACL injury in comparison with the normal population.[4] Previous cadaveric data supports that knee abduction loading increases in situ force of the ACL.[5] This indicates that the knee adduction-abduction moment reflects the ligament's stress and it can be used as a predictor of the athlete's risk for ACL injury.[4]

A common way to calculate the knee adduction-abduction moment is to use Newton-Euler's equation of motion. The equation consists of dynamic terms (inertia, Coriolis, and centrifugal force) and the external force term (moment of external force). In the landing motion that a large ground reaction force (GRF) suddenly applies at the impact foot, the contribution of the dynamic terms are considered to be negligible relative to the external force term. This suggests that the knee adduction-abduction moment can be approximated using only the external force term, i.e., the moment caused by the GRF. We call this simplified equa-

1) Mukogawa Women's University, Department of Health and Sports Sciences. *6-46 Ikebiraki, Nishinomiya, Hyogo 663-8558, JAPAN.*
2) University of Tsukuba, Comprehensive Human Sciences. *1-1-1 Tennodai, Tsukuba, Ibaraki 305-8577 JAPAN.*
Submitted for publication November 2013.
Accepted for publication February 2014.

tion of motion as "the external force model". The simplification of the equation of motion not only saves a computational cost to calculate dynamic terms but also provides a convenient estimate of the risk of the ACL injury.

One possible application of external force model would be a video analysis of ACL injury. Previous video analysis studies have mainly investigated the kinematic pattern of the injured knee joint.[3, 6-8] However, to know the true injury mechanism, it is essential to quantify the knee loads which actually caused the abnormal knee kinematics. If the GRF and its acting point are determined based on the kinematic data, the external force model will be able to extract the knee loading pattern from the video data.

The primary purpose of this study is to propose a external force model to predict the knee adduction-abduction moment aimed at establishing a convenient tool to determine the risk of ACL injury. The next objective is to verify the accuracy of the knee loading prediction based only on the kinematic data.

Ⅱ. Method

A. Model

1. Simplification of the equation of motion

Figure 1 (A) illustrates a right side leg model which involves the global Σ^O and shank Σ^S coordinate systems. All vectors in Fig. 1 (A) are represented in the global coordinate system Σ^O. The rotational equation of motion :

$$\boldsymbol{I}\ddot{\boldsymbol{\theta}} + \dot{\boldsymbol{\theta}} \times \boldsymbol{I}\dot{\boldsymbol{\theta}} = \boldsymbol{\tau} - \boldsymbol{J}^T\boldsymbol{f} \tag{1}$$

is usually used to analyze the dynamics of a link system, where $\boldsymbol{I}$ is the inertia matrix, $\boldsymbol{\theta}$ is the attitude of the segment, $\boldsymbol{\tau} = [\tau_x, \tau_y, \tau_z]^T$ is the joint moment, $\boldsymbol{J}$ is the Jacobian matrix and $\boldsymbol{f} = [f_x, f_y, f_z]^T$ is the GRF. The inertia term $\boldsymbol{I}\ddot{\boldsymbol{\theta}}$ and the gyroscopic torque $\dot{\boldsymbol{\theta}} \times \boldsymbol{I}\dot{\boldsymbol{\theta}}$ are moments derived from a rotational movement of a segment, and the external force term $\boldsymbol{J}^T\boldsymbol{f}$ is the moment caused by GRF. When the foot impacts the ground, the moment of GRF $\boldsymbol{J}^T\boldsymbol{f}$ becomes dominant compared to both the inertia term $\boldsymbol{I}\ddot{\boldsymbol{\theta}}$ and gyroscopic torque $\dot{\boldsymbol{\theta}} \times \boldsymbol{I}\dot{\boldsymbol{\theta}}$ as

$$\|\boldsymbol{I}\ddot{\boldsymbol{\theta}}\| \ll \|\boldsymbol{J}^T\boldsymbol{f}\|, \quad \|\dot{\boldsymbol{\theta}} \times \boldsymbol{I}\dot{\boldsymbol{\theta}}\| \ll \|\boldsymbol{J}^T\boldsymbol{f}\|. \tag{2}$$

We thus neglect the dynamic terms and obtain the externally applied knee moment $\hat{\boldsymbol{\tau}} = [\hat{\tau}_x, \hat{\tau}_y, \hat{\tau}_z]^T$ as

$$\hat{\boldsymbol{\tau}} = \boldsymbol{J}^T\boldsymbol{f}. \tag{3}$$

The Jacobian matrix is defined as

$$\boldsymbol{J} = [\boldsymbol{e}_x \times \boldsymbol{p}, \ \boldsymbol{e}_y \times \boldsymbol{p}, \ \boldsymbol{e}_z \times \boldsymbol{p}], \tag{4}$$

where unit vectors $\boldsymbol{e}_i \, (i = x, y, z)$ are the bases of the shank coordinate system Σ^S, which represent the knee rotation axes; $\boldsymbol{e}_x$ is the adduction-abduction axis pointing forward, $\boldsymbol{e}_y$ is the flexion-extension axis pointing medial, and $\boldsymbol{e}_z$ is the internal-external rotation axis pointing upward, respectively. The moment arm vector

$$\boldsymbol{p} = \boldsymbol{r}_c - \boldsymbol{r}_k \tag{5}$$

is the vector from knee joint center $\boldsymbol{r}_k = [r_{kx}, r_{ky}, r_{kz}]^T$ to the center of pressure (CoP) $\boldsymbol{r}_c = [r_{cx}, r_{cy}, r_{cz}]^T$. The knee adduction-abduction moment $\hat{\tau}_x$ can be extracted from Eq. (3) as

$$\begin{aligned} \hat{\tau}_x &= (\boldsymbol{e}_x \times \boldsymbol{p})^T \boldsymbol{f} \\ &= \|\boldsymbol{p}\| \boldsymbol{u}^T \boldsymbol{f}, \end{aligned} \tag{6}$$

where $\|\boldsymbol{p}\|$ is the length of the moment arm vector $\boldsymbol{p}$ and

$$\boldsymbol{u} = \frac{\boldsymbol{e}_x \times \boldsymbol{p}}{\|\boldsymbol{e}_x \times \boldsymbol{p}\|} \tag{7}$$

is the unit vector pointing medial and mutually perpendicular to $\boldsymbol{e}_x$ and $\boldsymbol{p}$. $\hat{\tau}_x$ in Eq. (6) is the knee adduction-abduction moment expressed in the shank coordinate system Σ^S, and a negative $\hat{\tau}_x$ denotes the knee abduction moment. The external force model (Eq. (6)) predicts the knee moment without angular accelerations, segmental masses, inertial moments and, moreover, segment by segment computations.

In addition, the external force model helps in understanding the principle of knee abduction moment generation. Since $\|\boldsymbol{p}\|$ is non-negative and nearly constant, $\boldsymbol{u}^T\boldsymbol{f}$ determines the direction and magnitude of knee adduction-abduction moment.

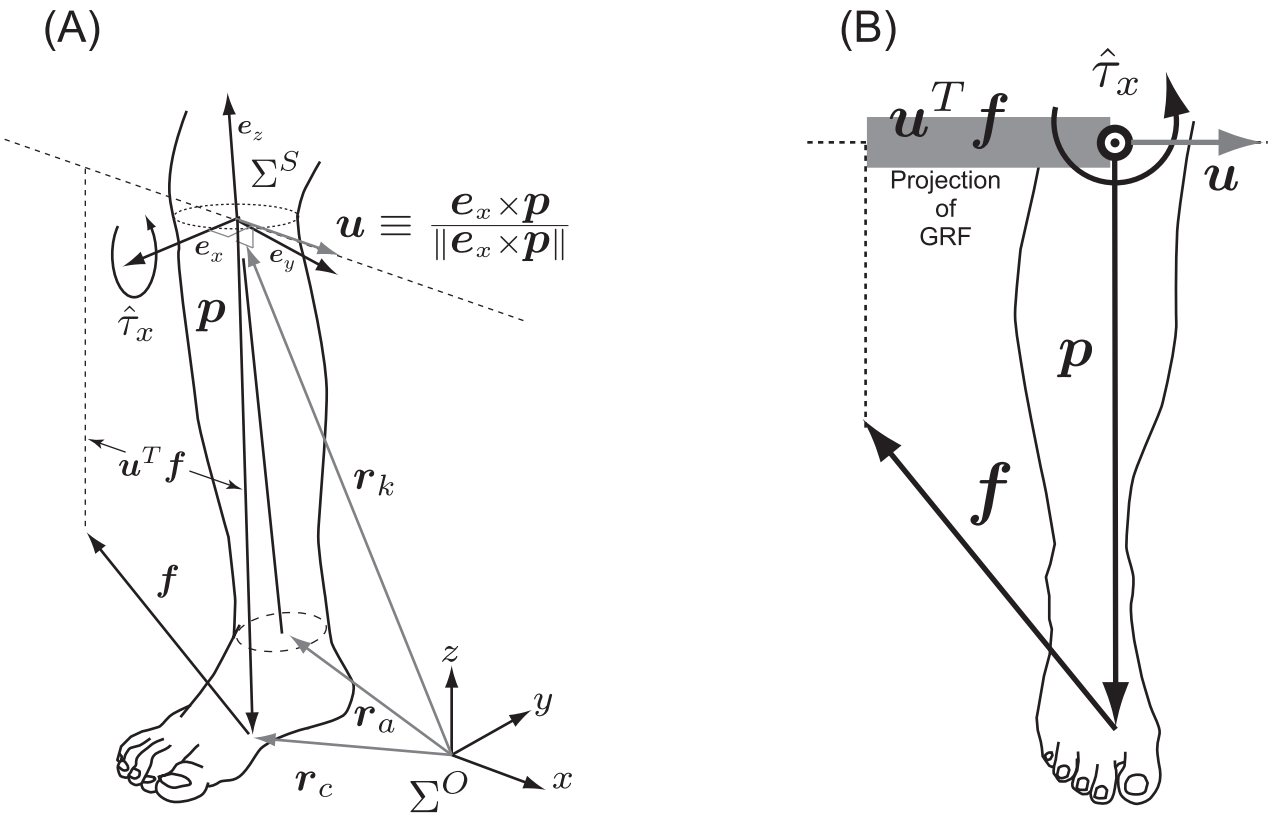

Figure 1: Schematic representation of the external force model

(A) The right side lower leg model. Σ^O and Σ^S denote the global and shank coordinates, respectively. $\hat{\tau}_x$ is the knee adduction-abduction moment acting about knee sagittal axis $\boldsymbol{e}_x$. The vector $\boldsymbol{p}$, which goes from knee joint center to center of pressure, represents moment arm. The vector $\boldsymbol{f}$ denotes ground reaction force. The vector $\boldsymbol{u}$ is the unit vector that is determined by orientations of both vector $\boldsymbol{p}$ and vector $\boldsymbol{e}_x$. The direction and the magnitude of the knee adduction-abduction moment is determined by $\boldsymbol{u}^T\boldsymbol{f}$; a projection of ground reaction force vector $\boldsymbol{f}$ onto the vector $\boldsymbol{u}$. The position vector of the center of ankle joint $\boldsymbol{r}_a$ was defined as the midpoint of the medial and lateral malleolus markers. The position vector of the center of knee joint $\boldsymbol{r}_k$ was defined as the midpoint of the medial and lateral femoral epicondyle markers. The internal-external rotation axis $\boldsymbol{e}_z$ was defined as a unit vector from the ankle joint center $\boldsymbol{r}_a$ to the knee joint center $\boldsymbol{r}_c$. The flexionextension axis $\boldsymbol{e}_y$ was defined as a unit vector which is medially pointing and mutually perpendicular to both $\boldsymbol{e}_z$ and a supplemental vector from the knee joint center $\boldsymbol{r}_c$ to the position of the marker on tibial tuberosity. Then the adduction-abduction axis $\boldsymbol{e}_x$ was defined by a cross product between $\boldsymbol{e}_y$ and $\boldsymbol{e}_z$.

(B) When GRF vector $\boldsymbol{f}$ directs laterally with respect to the moment arm vector $\boldsymbol{p}$, the knee moment becomes abduction.

$\boldsymbol{u}^T\boldsymbol{f}$ represents a projection of the GRF vector $\boldsymbol{f}$ onto the vector $\boldsymbol{u}$. When the acting line of the GRF $\boldsymbol{f}$ vector directs laterally with respect to the moment vector $\boldsymbol{p}$, then $\boldsymbol{u}^T\boldsymbol{f}$ increases in the negative direction and the knee moment becomes an abduction moment (Fig. 1 (B)). We suggest that the laterally directed GRF with respect to the moment arm vector $\boldsymbol{p}$ is the mechanism of knee abduction moment generation.

2. Estimation of GRF and its acting point from kinematic data

This section proposes models to estimate GRF and its acting point using measured kinematic data in the event that force plate data is unavailable. Assuming the body segments are rigid bodies, net force acting on the body is obtained by summing up translational equation of motion of all segments as

$$\hat{\boldsymbol{f}} = M(\ddot{\boldsymbol{c}} - \boldsymbol{g}), \tag{8}$$

where $M = \sum_{i=1}^{n} m_i$ is the total of each segmental mass m_i,

$$\boldsymbol{c} = \frac{1}{M}\sum_{i=1}^{n} m_i \boldsymbol{r}_i \tag{9}$$

is the position vector of body center of mass (CoM), $\boldsymbol{g} = [0, 0, -9.8]^T$ is the gravitational acceleration vector and $\boldsymbol{r}_i$ is the position vector of i^{th} segment's CoM. While standing with a single leg, if no other forces except for GRF are acting, then $\hat{\boldsymbol{f}}$ is assumed to be the GRF acting on stance foot. The acting point of GRF (CoP) was calculated by referring to the idea of zero-moment point (ZMP).[9] This idea suggests that ZMP coincides with CoP when the ground reaction forces and moments balance all the other forces and moments acting on the body. It also suggests that the horizontal components of the ground reaction moment vector $\boldsymbol{\tau}_p = [\tau_{px}, \tau_{py}, \tau_{pz}]^T$ acting at ZMP are always zero as

$$\boldsymbol{\tau}_p = [0, 0, \tau_{pz}]^T. \tag{10}$$

We thus obtain the position vector of ZMP $\boldsymbol{r}_z = [r_{zx}, r_{zy}, r_{zz}]^T$ from an equation of moment equilibrium by selecting a point at which horizontal components of the ground reaction moment vector, τ_{px} and τ_{py}, will be zero. The whole moment of the body $\boldsymbol{\tau}_{all}$ can be obtained by differentiating the angular momentum of the body $\boldsymbol{H}$ as

$$\boldsymbol{\tau}_{all} = \frac{d}{dt}\boldsymbol{H} = \boldsymbol{c} \times M\ddot{\boldsymbol{c}}. \tag{11}$$

The whole moment $\boldsymbol{\tau}_{all}$ is also expressed by sum of all the moments acting on the body as

$$\boldsymbol{\tau}_{all} = \boldsymbol{\tau}_g + \boldsymbol{\tau}_f, \tag{12}$$

where

$$\boldsymbol{\tau}_g = \boldsymbol{c} \times M\boldsymbol{g} \tag{13}$$

is the moment of gravity, and

$$\boldsymbol{\tau}_f = \boldsymbol{r}_z \times \boldsymbol{f} + \boldsymbol{\tau}_p \tag{14}$$

is the moment of GRF $\boldsymbol{f}$. Substituting Eq. (11), (13), and (14) into Eq. (12) gives

$$\boldsymbol{\tau}_p = \boldsymbol{c} \times M\ddot{\boldsymbol{c}} - \boldsymbol{c} \times M\boldsymbol{g} - \boldsymbol{r}_z \times \boldsymbol{f}. \tag{15}$$

We substitute the estimated GRF vector $\hat{\boldsymbol{f}}$ (Eq. (8)) into GRF vector $\boldsymbol{f}$ in Eq. (15) to obtain position vector of ZMP as

$$\boldsymbol{r}_z = \begin{bmatrix} c_x - \frac{c_z \ddot{c}_x}{\ddot{c}_z + g} \\ c_y - \frac{c_z \ddot{c}_y}{\ddot{c}_z + g} \\ 0 \end{bmatrix}. \tag{16}$$

3. The external force model with estimated GRF

Substituting estimated GRF $\hat{\boldsymbol{f}}$ (Eq. (8)) and ZMP $\boldsymbol{r}_z$ (Eq. (16)) into $\boldsymbol{f}$ in Eq. (6) and $\boldsymbol{r}_c$ in Eq. (5) respectively, we have the external force model with estimated GRF as

$$\begin{aligned} \check{\tau}_x &= \|\boldsymbol{r}_z - \boldsymbol{r}_k\| \hat{\boldsymbol{u}}^T \hat{\boldsymbol{f}} \\ &= M\|\hat{\boldsymbol{p}}\| \hat{\boldsymbol{u}}^T (\ddot{\boldsymbol{c}} - \boldsymbol{g}), \end{aligned} \tag{17}$$

where

$$\hat{\boldsymbol{p}} = \boldsymbol{r}_z - \boldsymbol{r}_k \tag{18}$$

is the moment arm vector taking account of ZMP and

$$\hat{\boldsymbol{u}} = \frac{\boldsymbol{e}_x \times \hat{\boldsymbol{p}}}{\|\boldsymbol{e}_x \times \hat{\boldsymbol{p}}\|} \tag{19}$$

is the unit vector that is pointing medial and perpendicular to both $\boldsymbol{e}_x$ and $\hat{\boldsymbol{p}}$.

B. Experiment

To verify the accuracy of the two external force models (Eq. (6) and Eq. (17)), we conducted a single-legged landing experiment and compared the results of these two solutions with that of the Newton–Euler method.

1. Subjects and protocol

Seven healthy adults (3 men: 25.0±1.0 yr, 172.3 ± 11.0cm, 68.2 ± 8.8kg, 4 women: 24.2 ± 0.5 yr, 161.7 ± 3.7cm, 56.2 ± 5.2kg), with no history of lower limb injuries, participated in this experiment. We explained the purpose of this research to the subjects and obtained written informed consent that was approved by the ethics committee of Japan Institute of Sports Sciences. After a 10 min warm up, we placed reflective markers on the subjects as shown in Fig. 2 and explained to them the experimental protocol that is detailed below.

Subjects were asked to fall from a 0.3 m high box and land on the force plate with their dominant leg. The dominant leg for each subject was

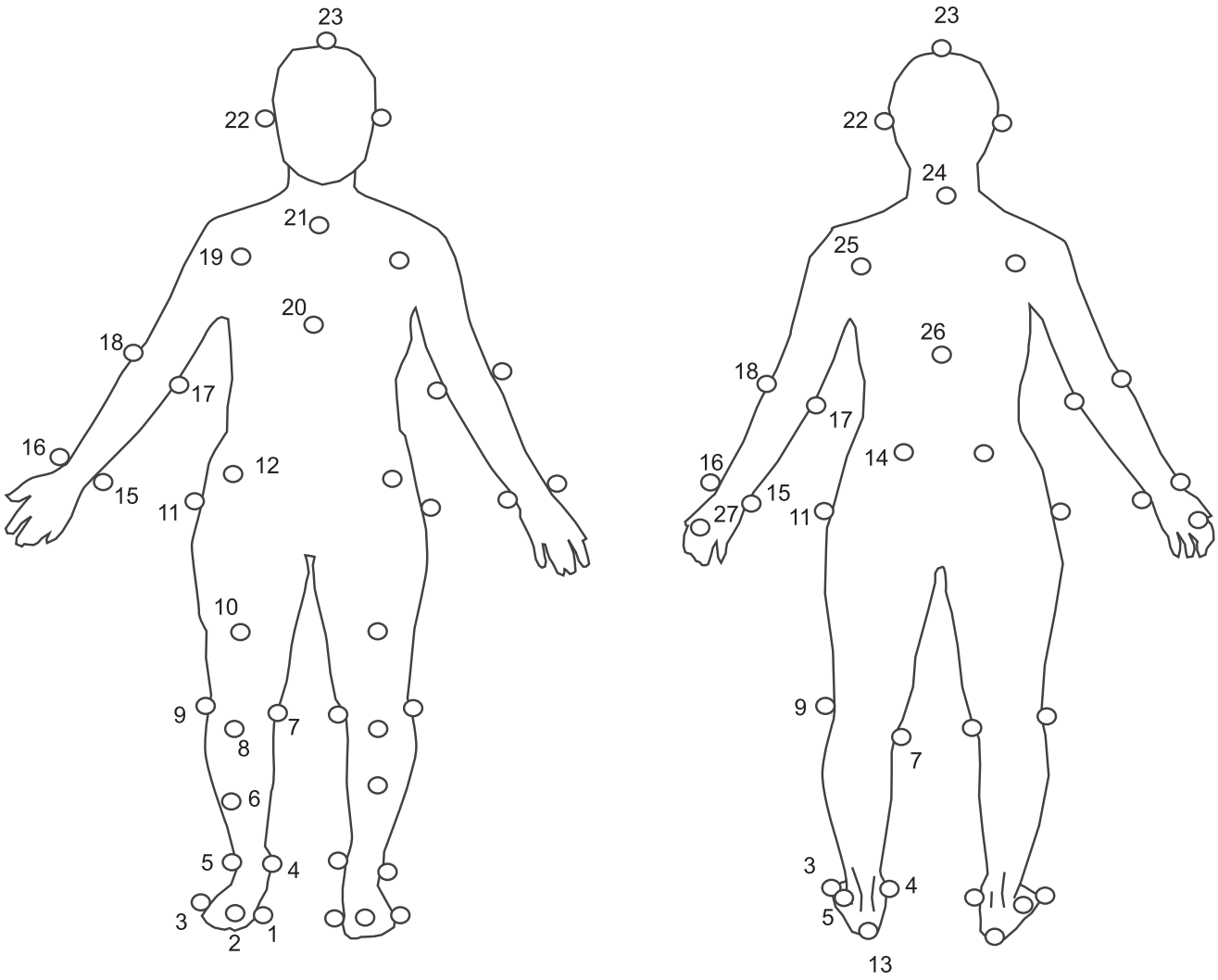

Figure 2: Position of the body markers

Reflective markers placed on following bony landmarks. (1) first metatarsophalangeal (MTP) joint, (2) second MTP joint, (3) fifth MTP joint, (4) tip of medial malleolus, (5) tip of lateral malleolus, (6) anterior aspect of shank, (7) the most medial point of the border of the medial femoral epicondyle, (8) the center of tibial tuberosity, (9) the most lateral point of the border of the lateral femoral epicondyle, (10) anterior aspect of thigh, (11) tip of great trochanter, (12) anterior superior iliac spine, (13) the most posterior point of the heel, (14) posterior superior iliac spine, (15) ulnar styloid process, (16) radial styloid process, (17) medial epicondyle of humerus, (18) lateral epicondyle of humerus, (19) anterior aspect of the shoulder joint, (20) the most inferior edge of the sternum, (21) mid point of bilateral sternoclavicular joint, (22) in front of the ear, (23) tip of the head, (24) C7 spinous process, (25) posterior aspect of the shoulder joint, (26) T10 spinous process and (27) mid point of the third metacarpal bone.

determined as the leg that was usually used to kick a ball. No further instructions were provided. Trials in which a subject was able to maintain a single leg stance for two seconds were regarded as successful. A maximum of 56 trials per subject were carried out, with 3 minutes of rest after every 10 trials to avoid fatigue.

C. Data acquisition and analysis

The positions of the reflective markers were captured with a Vicon 624 system (Oxford Metrics, Oxford, UK) at a sampling frequency of 120 Hz. The GRF data was measured by the force plate (9287B, Kistler, Winterthur, Switzerland) synchronously with the kinematic data. Trials with more than 20 consecutive frame gaps were excluded. The position data of the reflective markers

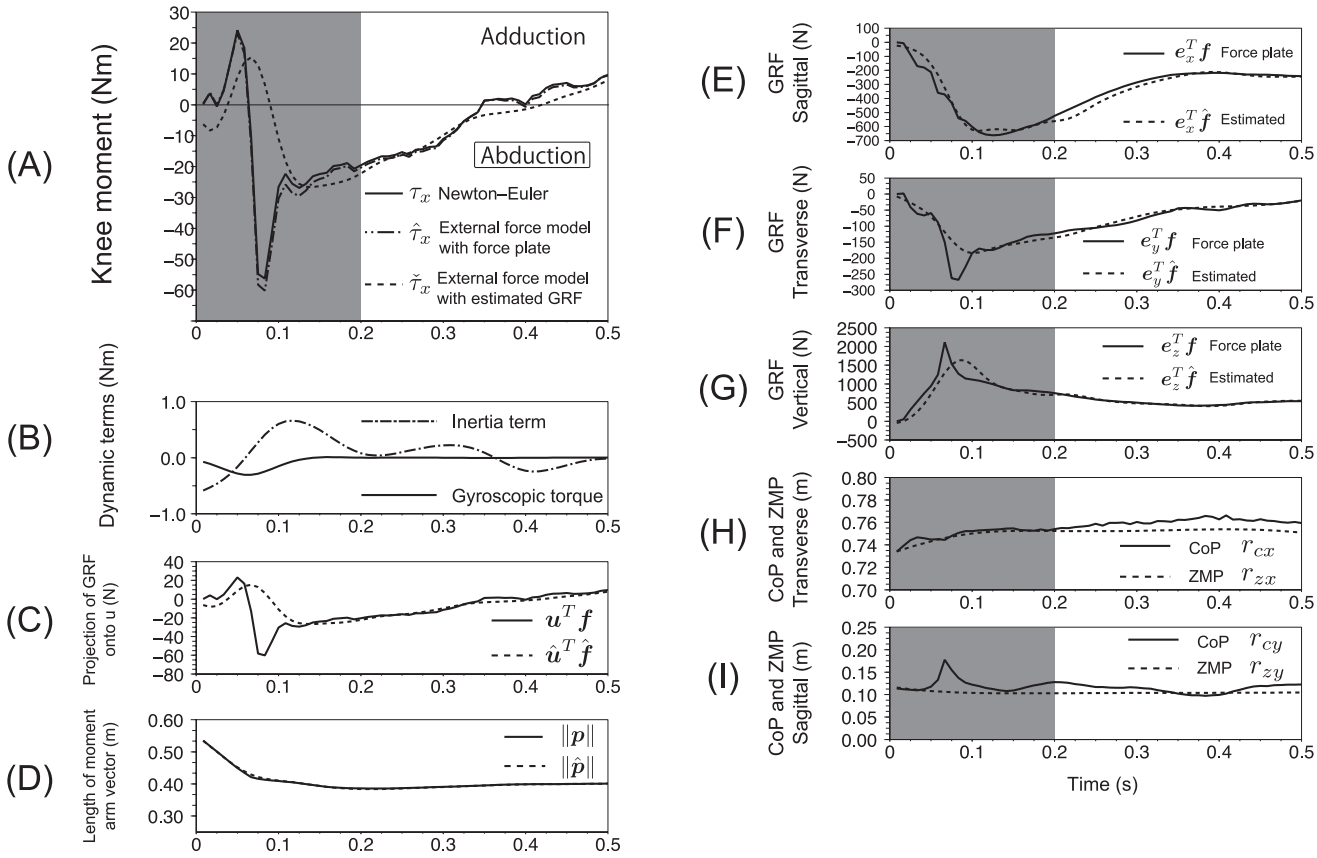

Figure 3: Time histories of knee moment, dynamic terms, external force term, moment arm length, estimated GRF, and ZMP.

A time history of the knee joint moment, GRF and ZMP from a representative subject. (A) Comparison of the knee adduction-abduction moment (Newton–Euler method τ_x: solid line, the external force model using force plate data (Eq. (6)) $\hat{\tau}_x$: dashed spaced line, and the external force model using estimated GRF (Eq. (17)) $\check{\tau}_x$: dashed line). (B) Dynamic terms of equation of motion. Both torques are acting about the knee adduction-abduction axis $\boldsymbol{e}_x$ (C) Projection of the GRF vector onto the vector $\boldsymbol{u}$. (D) Length of the moment arm vector. (E–G) Comparison of the force plate (solid line) and estimated GRF (dashed line), expressed in the shank coordinate system Σ^S. (H, I) Comparison of measured CoP by force plate (solid line) and calculated ZMP from kinematic data (dashed line). The gray shaded areas represent the periods analyzed with RMSE and % RMSE.

were smoothed using a low-pass second order zero lag Butterworth digital filter at cut-off frequencies of 10 Hz for the transverse and sagittal components and 18 Hz for the vertical component. Cut-off frequencies were determined to minimize the root mean square error (RMSE) between the estimated GRF (Eq. (8)) and force plate data.[10] Using the measured kinematic and force plate data, the knee adduction-abduction moments based on different solutions (τ_x: Newton–Euler method, $\hat{\tau}_x$: the external force model with force plate data (Eq. (6)) and $\check{\tau}_x$: the external force model with estimated GRF (Eq. (17))) were calculated. The anthropometric parame- ters were estimated based on[11] for the inverse dynamics calculation with the Newton–Euler method. $\hat{\tau}_x$ and $\check{\tau}_x$ were compared with τ_x to verify the accuracies of each external force model. The estimated GRF $\hat{\boldsymbol{f}}$ and ZMP $\boldsymbol{r}_z$ were compared with the force plate data. The errors between different solutions were quantified using the RMSE and relative RMSE (% RMSE).[12] The time window of interest was defined from 0 to 0.2 s after the initial foot impact.

Ⅲ. Results

A. Accuracy of the external force model

Figure 3 (A) compares the moment of the Newton-Euler method (solid line) and those of two external force models; one using the force plate data (dashed spaced line) and the other using the estimated GRF (dashed line). The external force model with force plate data showed a good prediction with small % RMSE of 2.12±1.1 % and RMSE of 1.71±1.0 Nm. Figure 4 (A) shows the relationship between $\hat{\tau}_x$ and τ_x from all 295 trials at each 0.05 s steps from 0.05 to 0.2 s after foot impact. This figure also shows that $\hat{\tau}_x$ linearly correlates with τ_x throughout the investigated period. Figure 3 (B) illustrates the time histories of the dynamic terms of the same trial. The small amplitudes of these dynamic terms indicate that the external force term of the equation of motion mainly determines the magnitude of the knee adduction-abduction moment. Figure 3 (C) shows the time profile of $\boldsymbol{u}^T\boldsymbol{f}$ and $\hat{\boldsymbol{u}}^T\hat{\boldsymbol{f}}$, and Fig. 3 (D) represents the length of the moment arm vectors $\boldsymbol{p}$ and $\hat{\boldsymbol{p}}$. Both $\boldsymbol{u}^T\boldsymbol{f}$ and $\hat{\boldsymbol{u}}^T\hat{\boldsymbol{f}}$ show profiles similar to those of τ_x and $\hat{\tau}_x$, respectively. The length of the moment arm vectors was nearly constant throughout the period of interest, except for a small shortening due to ankle dorsiflexion in the early phase. These results indicated that the direction and magnitude of each knee adduction-abduction moment (τ_x and $\hat{\tau}_x$) are mainly determined by the external forces $\boldsymbol{u}^T\boldsymbol{f}$ and $\hat{\boldsymbol{u}}^T\hat{\boldsymbol{f}}$, respectively. The moment calculated by the external force model using the estimated GRF (Eq. (17)) indicated less accurate results (% RMSE of 24.1±7.6 % and RMSE of 19.3±8.4 Nm) than when using the force plate data. The time pattern of moment $\check{\tau}_x$ did not follow the sudden change of the moment τ_x calculated by the Newton-Euler method in the early phase (Fig. 3 (A)). The poor accuracy in the early phase is also obvious in the correlation coefficients between $\check{\tau}_x$ and τ_x that were the smallest at 0.05 s (R = 0.90) and were gradually increased as time passed by (Fig. 4 (B)).

B. GRF and ZMP calculation from kinematic data

Figure 3 (E) - (G) compares the estimated GRF $\hat{\boldsymbol{f}}$ with the force plate data $\boldsymbol{f}$. The general trend of each component broadly agreed with the force plate data; however, the impact force in the early phase cannot be estimated in every component and large errors were obtained (RMSE

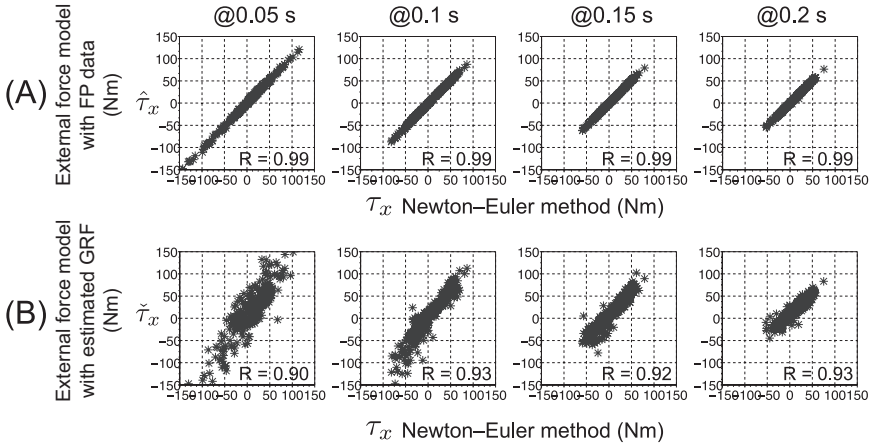

Figure 4: Association between each external force model and the Newton-Euler method.

(A) Association between the knee moment calculated by the external force model with force plate data and that of the Newton-Euler method. (B) Association between the knee moment calculated by the external force model with estimated GRF and that of the Newton-Euler method. Every plot was based on data from all 295 trials of every subject at each 0.05 s steps from 0 to 0.2 s after foot impact. The external force model showed a good prediction throughout the investigated period; however, when using the estimated GRF, less accurate estimates were obtained in the early phase.

Transverse: 26.6±17.5 N, Sagittal: 66.3±19.4 N, and Vertical: 149.2±64.5 N, % RMSE Transverse: 19.7±3.7 %, Sagittal: 19.9±3.1 %, and Vertical: 8.3±2.1%).

Figures 3 (H) and (I) compare the patterns of ZMP and CoP during the same trial. Although the resulting % RMSEs values were large (36.4±14.8 % for transverse and 61.5±28.1 % for sagittal component) due to ZMP's small value, the absolute errors (0.01±0.01 m for transverse and 0.04±0.02 m for sagittal) were reasonably small to allow substitution of the CoP.

Ⅳ. Discussion

A. Accuracy of the external force models

The purpose of this study was to propose a simple method to evaluate the knee loading pattern during impact phase using the external force model. The experimental results indicated that the moment calculated by the external force model using the force plate data (Eq. (6)) strongly agreed with the moment calculated by the Newton–Euler method, despite the fact that the external force model neglects the dynamic terms of the equation of motion. This indicates that the knee adduction-abduction moment is largely determined by the external force (GRF), which is highly increased just after foot impact.

The benefits of the external force model include not only reducing computational costs or avoiding recursive calculations but also eliminating the influence of numerical noises which are accumulated in the differential process.

Moreover, this model provide a insight into decreasing the risk of ACL injury. As Fig. 1 (B) and Fig 3 (A) shows, the knee adduction-abduction is increased as the magnitude of $\boldsymbol{u}^T\boldsymbol{f}$ increased. Therefore, to minimize knee abduction loading and

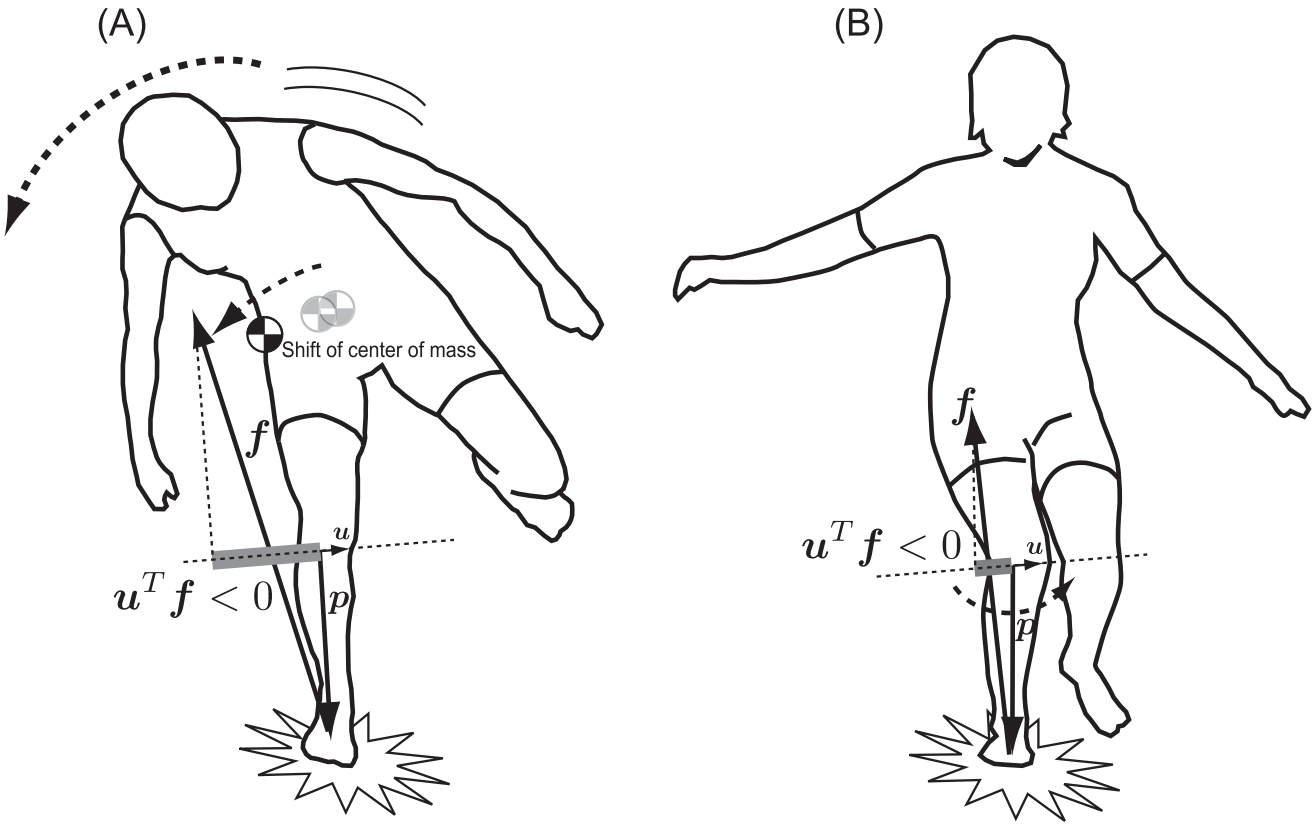

Figure 5: Risk elevating landing postures

Examples of landing postures that potentially increase the knee abduction moment. The lateral shift of the body CoM toward the landing limb (A) or medially positioned lower shank (B) experience increased knee abduction moment. To reduce the risk of ACL injury, one should avoid these landing postures.

to prevent ACL injuries, a great care should be taken to align landing leg orientation relative to the direction of GRF so as to minimize the magnitude of $\boldsymbol{u}^T\boldsymbol{f}$.

One possible application of the external force model is to analyze the injury video data, and determine how large the knee abduction moment occurred at the moment of injury. However, the force plate data is usually unavailable in the actual sports games. This study hence attempted to estimate GRF using kinematic data aimed at future application of the external force model to injury video analysis. The results indicated that the knee adduction-abduction moment calculated by the external force model using estimated GRF (Eq. (17)) broadly agreed with that calculated by the Newton–Euler method. However it was less accurate than that calculated using force plate data because the GRF model (Eq. (8)) cannot predict impact force in the early phase. This result suggested that it is difficult to estimate impact force only with the measured kinematic data. The ACL injury is reported to occur 13–105 ms after impact[2] and its time duration overlaps with that of the impact force. The precise estimates of GRF in impact phase is therefore required to yield accurate risk evaluation. The impact force, i.e., high frequency force in time histories in GRF[13] is generated by the foot collision with the ground; previous studies have estimated the time pattern of impact force using mass-spring-damper models.[14–16] At this point, our model does not include such mathematical approach and this is recognized as a substantial limitation for the current model which are going to analyze the impact phase of ACL injury. Future studies should add a spring and damper terms into current model to achieve more sensitive prediction of the impact induced knee moment.

Although large RMSEs were expected in predicting ZMP due to the acceleration of the body CoM, a practical accuracy was obtained. One limitation of the current ZMP model is that it cannot distinguish between more than two force acting points. Our approach cannot investigate the ACL injury during bilateral landing or that involving body contacts from other players because the acting point of GRF on injured leg becomes indeterminable. The contact force cannot be obtained as well in the latter case. Hence it is noted that the current external force model using ZMP is feasible only for single stance and non-contact ACL injury.

B. Clinical implications

In addition to the aspect of risk screening, the external force model is helpful to understand how the knee abduction moment occurs. We can suggest that the following landings increase the knee abduction moment. First, a lateral shift of the body CoM toward the landing limb, which allows the GRF to direct laterally with respect to the vector $\boldsymbol{p}$ (Fig. 5 (A)). This kind of landing posture occurs due to the trunk leaning toward the landing limb.[3] Secondly, the medially positioned shank with respect to the acting line of the GRF will also increase the knee abduction moment (Fig. 5 (B)). Such a limb position is observed in real injury situations.[3] Our model suggests that these kinds of motions and limb positions should be avoided to reduce the risk of ACL injury.

Conflict of interest

None of the authors have conflict of interests.

Acknowledgements

This research was partially supported by the Ministry of Education, Science, Sports, and Culture, Grant-in-Aid for Young Scientists (B), 21700667, 2009. We would like to thank Yohei CHIBA and Megumi ARAKI for their assistance in experiment and data processing.

References

1. Ireland ML. Anterior cruciate ligament injury in female athletes: Epidemiology. J Athl Train, 34 (2), 150–154, 1999.
2. Krosshaug T, Nakamae A, Boden BP, et al. Mecha-

nisms of anterior cruciate ligament injury in basketball: video analysis of 39 cases. Am J Sports Med, 35 (3), 359–367, 2007.
3. Olsen OE, Myklebust G, Engebretsen L, et al. Injury mechanisms for anterior cruciate ligament injuries in team handball: a systematic video analysis. Am J Sports Med, 32 (4), 1002–1012, 2004.
4. Hewett TE, Myer GD, Ford KR, et al. Biomechanical measures of neuromuscular control and valgus loading of the knee predict anterior cruciate ligament injury risk in female athletes: a prospective study. Am J Sports Med, 33 (4), 492–501, 2005.
5. Markolf KL, Burchfield DM, Shapiro MM, et al. Combined knee loading states that generate high anterior cruciate ligament forces. J Orthop Res, 13 (6), 930–935, 1995.
6. Hewett TE, Torg JS, and Boden BP. Video analysis of trunk and knee motion during non-contact anterior cruciate ligament injury in female athletes: lateral trunk and knee abduction motion are combined components of the injury mechanism. Br J Sports Med, 43 (6), 417–422, 2009.
7. Krosshaug T and Bahr R. A model-based image-matching technique for three-dimensional reconstruction of human motion from uncalibrated video sequences. J Biomech, 38 (4), 919–929, 2005.
8. Krosshaug T, Slauterbeck JR, Engebretsen L, et al. Biomechanical analysis of anterior cruciate ligament injury mechanisms: three-dimensional motion reconstruction from video sequences. Scand J Med Sci Sports, 17 (5), 508–519, 2007.
9. Vukobratovic M. Zero-moment point thirty five years of its life. International Journal of Humanoid Robotics, 1, 157–173, 2004.
10. Ren L, Jones RK, and Howard D. Whole body inverse dynamics over a complete gait cycle based only on measured kinematics. J Biomech, 41 (12), 2750–2759, 2008.
11. Chandler RF, Clauser CE, McConville JT, et al. Investigation of inertial properties of the human body. Aerospace medical research laboratory technical report, pages 74–137, 1975.
12. Kuo AD. A least-squares estimation approach to improving the precision of inverse dynamics computations. J Biomech Eng, 120 (1), 148–159, 1998.
13. Bobbert MF, Schamhardt HC, and Nigg BM. Calculation of vertical ground reaction force estimates during running from positional data. J Biomech, 24 (12), 1095–1105, 1991.
14. Zadpoor AA, Nikooyan AA, and Arshi AR. A model-based parametric study of impact force during running. J Biomech, 40 (9), 2012–2021, 2007.
15. Liu W and Nigg BM. A mechanical model to determine the influence of masses and mass distribution on the impact force during running. J Biomech, 33 (2), 219–224, 2000.
16. Nigg BM and Liu W. The effect of muscle stiffness and damping on simulated impact force peaks during running. J Biomech, 32 (8), 849–856, 1999.